

## 192906: mafic granulite, Burngup

(*Youanmi Terrane, Yilgarn Craton*)

Blereau, ER, Korhonen, FJ and Kelsey, DE

### Location and sampling

NEWDEGATE (SI 50-8), BURNGUP (2631)

MGA Zone 50, 657027E 6345359N

Warox Site FJKBGD192906

Sampled on 20 May 2009

This sample was collected from an outcrop in a field, about 12.5 km west-southwest of Sheoak Hill, and 0.8 km west of Burngup townsite, and 0.2 km immediately south of Biddy Camm Road. The sample was collected as part of the Yilgarn Craton Metamorphic Project (2003–14) undertaken by Ben Goscombe for the Geological Survey of Western Australia (GSWA), and referred to in that study as sample BG09-153. The results from this project have not been released by GSWA, although select data have been published in Goscombe et al. (2019). This sample is not available in the GSWA collections; all observations are based on descriptions presented in Goscombe et al. (2019) and have not been directly verified.

### Geological context

The unit sampled is a mafic granulite of the western Youanmi Terrane (Quentin de Gromard et al., 2021). This unit is part of a belt of Archean metasedimentary and gneissic rocks previously assigned to the South West Terrane and referred to informally by Wilde and Pidgeon (1987) as the ‘Wheat Belt’ region (cf. Wilde, 2001). However, a recent reinterpretation places the boundary between the South West and the Youanmi Terranes farther to the southwest than shown on older maps (Quentin de Gromard et al., 2021). The Youanmi Terrane contains both granite–greenstone and high-grade gneiss components with emplacement ages from 3010 to 2600 Ma (GSWA, 2020; Cassidy et al., 2006). Existing geochronological data from this part of the Youanmi Terrane is sparse. A biotite metagranodiorite, collected about 127 km to the southeast of this locality, yielded an igneous crystallization age of  $2978 \pm 5$  Ma (GSWA 224357, Lu et al., 2018). Two samples of garnet-bearing alkali feldspar granite from Griffins Find approximately 34 km to the west-southwest yielded crystallization ages of c. 2636 Ma (Qiu and McNaughton, 1999). A quartzite also collected from Griffins Find yielded detrital zircon dates between c. 3812 and 2643 Ma, and a conservative maximum age of deposition of  $2655 \pm 11$  Ma (GSWA 198580, Lu et al., 2015b). A pelitic gneiss from Griffins Find yielded detrital zircon dates between c. 2838 and 2629 Ma, and a conservative maximum depositional age of  $2638 \pm 2$  Ma (GSWA 198578, Lu et al., 2015a), and another pelitic gneiss sample yielded a monazite age for high-grade metamorphism of  $2641 \pm 6$  Ma (GSWA 198585, Fielding et al., 2021).

### Petrographic description

The sample is a massive medium-grained mafic granulite containing green–brown hornblende, plagioclase, clinopyroxene, orthopyroxene and minor quartz (Fig. 1). Clinopyroxene is zoned with Al-bearing augite cores and diopside-rich rims. The presence of biotite, K-feldspar and Fe–Ti oxides have not been noted. The sample has a granoblastic matrix with diffuse banding on a 1–2 mm scale. Mineral compositions are provided in Table 1.

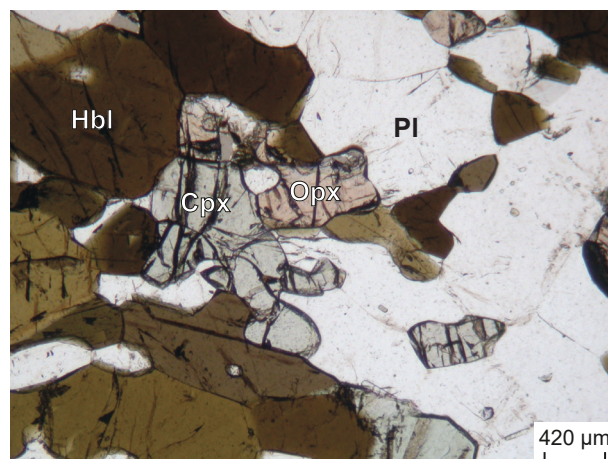


**Figure 1.** Photomicrograph of sample 192906: mafic granulite, Burngup in plane-polarized light. Mineral abbreviations are explained in the caption to Figure 2

**Table 1. Mineral compositions for sample 192906: mafic granulite, Burngup**

Mineral <sup>(a)</sup>	Hbl	Hbl	Cpx	Cpx	Pl	Pl	Opx	Opx
Setting	Core	Rim	Core	Rim	Core	Rim	Core	Rim
<i>wt%</i>								
SiO <sub>2</sub>	43.10	43.98	51.32	51.54	56.55	55.36	51.41	51.38
TiO <sub>2</sub>	2.49	2.33	0.16	0.20	0.00	0.02	0.14	0.10
Al <sub>2</sub> O <sub>3</sub>	10.40	10.33	1.47	1.07	26.53	26.75	0.93	0.73
Cr <sub>2</sub> O <sub>3</sub>	0.00	0.00	0.00	0.00	0.00	0.00	0.00	0.00
FeO	17.22	16.47	11.94	11.49	0.13	0.38	29.46	29.63
MnO	0.19	0.17	0.31	0.28	0.00	0.01	0.72	0.73
MgO	9.90	10.02	12.33	12.67	0.00	0.04	16.60	16.58
ZnO	0.08	0.00	0.00	0.00	0.05	0.03	0.00	0.07
CaO	11.10	11.24	21.21	21.71	9.81	10.32	0.76	0.69
Na <sub>2</sub> O	1.63	1.52	0.36	0.35	5.75	5.64	0.02	0.00
K <sub>2</sub> O	1.25	1.17	0.00	0.03	0.36	0.31	0.00	0.01
Total <sup>(b)</sup>	97.34	97.23	99.11	99.32	99.17	98.86	100.03	99.92
Oxygen	23	23	6	6	8	8	6	6
Si	6.44	6.55	1.95	1.95	2.57	2.52	1.99	1.99
Ti	0.28	0.26	0.00	0.01	0.00	0.00	0.00	0.00
Al	1.83	1.81	0.07	0.05	1.42	1.44	0.04	0.03
Cr	0.00	0.00	0.00	0.00	0.00	0.00	0.00	0.00
Fe <sup>3+(c)</sup>	0.58	0.47	0.05	0.07	0.00	0.00	0.00	0.00
Fe <sup>2+</sup>	1.58	1.58	0.33	0.30	0.00	0.01	0.95	0.96
Mn <sup>2+</sup>	0.02	0.02	0.01	0.01	0.00	0.00	0.02	0.02
Mg	2.20	2.23	0.70	0.72	0.00	0.00	0.96	0.96
Zn	0.01	0.00	0.00	0.00	0.00	0.00	0.00	0.00
Ca	1.78	1.79	0.86	0.88	0.48	0.50	0.03	0.03
Na	0.47	0.44	0.03	0.03	0.51	0.50	0.00	0.00
K	0.24	0.22	0.00	0.00	0.02	0.02	0.00	0.00
Total	15.43	15.38	4.00	4.00	5.00	5.00	4.00	4.00
<i>Compositional variables<sup>(d)</sup></i>								
y(Opx)	—	—	—	—	—	—	0.03	0.03
XFe	0.42	0.42	0.32	0.29	—	—	0.50	0.50

**NOTES:** — not applicable

(a) Mineral abbreviations explained in the caption to Figure 2

(b) Totals on anhydrous basis

(c) Hornblende cations calculated following Holland and Blundy (1994); Fe<sup>3+</sup> contents for other minerals based on Droop (1987)

(d) y(Opx) = Al on the M1 site (White et al., 2014); XFe = Fe<sup>2+</sup>/(Fe<sup>2+</sup> + Mg)

## Analytical details

Preliminary  $P$ – $T$  estimates were obtained using multiple-reaction and conventional thermobarometry calculated from the mineral compositions (Table 1). These estimates were derived from the ‘averagePT’ module (avPT) in the program THERMOCALC version tc325 (Powell and Holland, 1988), using the internally consistent Holland and Powell (1998) dataset.

The metamorphic evolution of this sample has been subsequently re-evaluated using phase equilibria modelling, based on the bulk-rock composition (Table 2). The bulk-rock composition was determined by X-ray fluorescence spectroscopy, together with loss on ignition (LOI). The modelled O content (for  $\text{Fe}^{3+}$ ) was set to be 20% of the measured total Fe. The  $\text{H}_2\text{O}$  content derived from the measured LOI did not reproduce the observed hornblende-bearing assemblage, therefore the  $\text{H}_2\text{O}$  content was modified to calculate the approximate mode of hornblende (10–15 mol%). The bulk composition was also adjusted for the presence of apatite by applying a correction to CaO (Table 2). Thermodynamic calculations were performed in the NCKFMASHTO ( $\text{Na}_2\text{O}$ – $\text{CaO}$ – $\text{K}_2\text{O}$ – $\text{FeO}$ – $\text{MgO}$ – $\text{Al}_2\text{O}_3$ – $\text{SiO}_2$ – $\text{H}_2\text{O}$ – $\text{TiO}_2$ – $\text{O}$ ) system using THERMOCALC version tc340 (Powell and Holland, 1988; updated October 2013) and the internally consistent thermodynamic dataset of Green et al. (2016; version dataset tc-ds63, created January 2015). The activity–composition relations used in the modelling are detailed in Green et al. (2016), with the augite model used for clinopyroxene. Compositional and mode isopleths for all phases were calculated using the software TCIInvestigator (Pearce et al., 2015). Additional information on the workflow with relevant background and methodology are provided in Korhonen et al. (2020).

**Table 2.** Measured whole-rock and modelled compositions for sample 192906: mafic granulite, Burngup

<i>XRF whole-rock composition (wt%)<sup>(a)</sup></i>												
$\text{SiO}_2$	$\text{TiO}_2$	$\text{Al}_2\text{O}_3$	$\text{Fe}_2\text{O}_3^{(b)}$	$\text{FeO}^{(b)}$	$\text{MnO}$	$\text{MgO}$	$\text{CaO}$	$\text{Na}_2\text{O}$	$\text{K}_2\text{O}$	$\text{P}_2\text{O}_5$	LOI	Total
56.37	0.64	10.88	11.62	10.47	0.17	6.14	8.59	2.49	0.42	0.04	<0.01	107.83
<i>Normalized composition used for phase equilibria modelling (mol%)</i>												
$\text{SiO}_2$	$\text{TiO}_2$	$\text{Al}_2\text{O}_3$	$\text{O}^{(c)}$	$\text{FeO}^{(d)}$	$\text{MnO}$	$\text{MgO}$	$\text{CaO}^{(e)}$	$\text{Na}_2\text{O}$	$\text{K}_2\text{O}$	–	$\text{H}_2\text{O}^{(f)}$	Total
60.09	0.51	6.83	0.84	8.40	–	9.75	9.74	2.57	0.29	–	1.00	100

**NOTES:** (a) Data and analytical details are available from the WACHEM database <<http://geochem.dmp.wa.gov.au/geochem/>>  
 (b) FeO content is total Fe  
 (c) O content (for  $\text{Fe}_2\text{O}_3$ ) set to be 20% of measured  $\text{FeO}^{(b)}$   
 (d)  $\text{FeO}^{\text{T}}$  = moles  $\text{FeO}$  + 2 \* moles O  
 (e) CaO modified to remove apatite:  $\text{CaO}(\text{Mod}) = \text{CaO}(\text{Total}) - (\text{moles CaO}(\text{in Ap}) = 3.33 * \text{moles P}_2\text{O}_5)$   
 (f)  $\text{H}_2\text{O}$  content adjusted to reproduce approximate mode of hornblende (10–15 mol%)  
 – not applicable

## Results

The  $P$ – $T$  pseudosection for sample 192906 was calculated over a  $P$ – $T$  range of 2–10 kbar and 660–900 °C (Fig. 2). The solidus is located between 765 and 880 °C across the range of modelled pressures. Magnetite has a maximum pressure stability of 5.1 kbar at 600 °C over the range of modelled conditions. Rutile is stable above 8.0 kbar at 600 °C, which extends to higher pressure with increasing temperature. Garnet is stable at pressures above 5.4 kbar at 600 °C and above 9.3 kbar at 900 °C. Biotite is stable at temperatures below 820 °C at 5.7 kbar and below 690 °C at 6.6 kbar.

Metamorphic  $P$ – $T$  estimates ( $\pm 2\sigma$  uncertainty) calculated using multiple-reaction thermobarometry are  $4.2 \pm 3.3$  kbar and  $800 \pm 73$  °C. These calculations used the core compositions (Table 1) to estimate peak conditions. Conventional thermobarometry using the orthopyroxene–clinopyroxene and hornblende–clinopyroxene thermometers and Al-in-hornblende barometer reportedly yield results of 785–820 °C and  $5.2 \pm 0.4$  kbar (Goscombe et al., 2019).

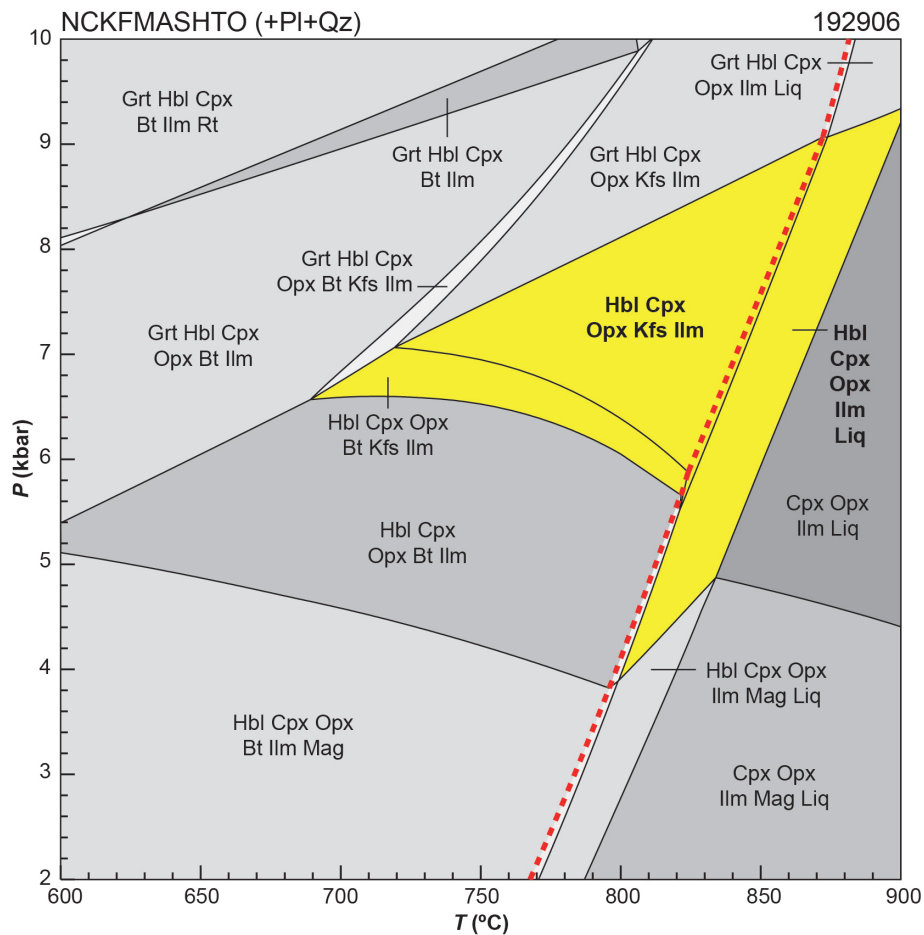


**Figure 2.** *P*–*T* pseudosection calculated for sample 192906: mafic granulite, Burngup. Assemblage fields corresponding to peak metamorphic conditions are delimited by bold text and yellow shading. Red dashed line represents the solidus. Abbreviations: Bt, biotite; Cpx, clinopyroxene; Grt, garnet; Hbl, hornblende; Ilm, ilmenite; Kfs, K-feldspar; Liq, silicate melt; Mag, magnetite; Opx, orthopyroxene; Pl, plagioclase; Qz, quartz; Rt, rutile

## Interpretation

The observed mineral assemblage consists of hornblende, clinopyroxene, orthopyroxene, plagioclase and quartz. Given these constraints, the peak metamorphic assemblage is interpreted to be hornblende–clinopyroxene–orthopyroxene–plagioclase–ilmenite–quartz(–K-feldspar–biotite–melt). There is uncertainty whether the sample has undergone partial melting or whether K-feldspar or biotite could be present in the sample but were misidentified. The subsolidus hornblende–clinopyroxene–orthopyroxene–K-feldspar–plagioclase–ilmenite–quartz field is stable between 720 and 870 °C at 5.9 – 8.8 kbar. The suprasolidus hornblende–clinopyroxene–orthopyroxene–plagioclase–ilmenite–quartz–melt field is stable between 800 and 900 °C at 3.9 – 9.3 kbar. The stability of both assemblages is delimited by the presence of garnet at higher pressures, the growth of biotite at lower pressures and temperatures, and the loss of hornblende at higher temperatures.

Within the subsolidus hornblende–clinopyroxene–orthopyroxene–K-feldspar–plagioclase–ilmenite–quartz field, up to 1.4 mol% (approximately equivalent to vol%) K-feldspar is predicted at 720 °C, decreasing with increasing temperature until K-feldspar is consumed at the solidus (Fig. 3a). Given this low amount of K-feldspar, it is not possible to use its inferred absence in thin section as a reliable constraint. At lower *P*–*T* conditions, up to 2 mol% biotite is predicted in the hornblende–clinopyroxene–orthopyroxene–biotite–K-feldspar–plagioclase–ilmenite–quartz field, increasing up to 3 mol% in the hornblende–clinopyroxene–orthopyroxene–biotite–plagioclase–ilmenite–quartz field at lower pressures (Fig. 3b). Biotite is not described in the sample, supporting the interpretation that peak conditions were outside the stability of biotite or close to the biotite-out line. Up to 6 mol% melt is predicted in the suprasolidus hornblende–clinopyroxene–orthopyroxene–plagioclase–ilmenite–quartz–melt field (Fig. 3c), although textural evidence to support the presence of former melt cannot be verified.

The metamorphic  $P$ – $T$  estimates calculated using multiple-reaction thermobarometry have significant uncertainties and offer no meaningful constraints. The results from conventional thermobarometry mainly fall within the hornblende–clinopyroxene–orthopyroxene–biotite–plagioclase–ilmenite–quartz field, extending into the lower pressure limit of the hornblende–clinopyroxene–orthopyroxene–plagioclase–ilmenite–quartz–melt field at higher temperature. Although it is well established that many minerals will not retain peak granulite facies compositions, the Al content in orthopyroxene has long been recognised as a more reliable indicator of high-temperature metamorphism in metasedimentary rocks (e.g. Fitzsimons and Harley, 1994; Pattison et al., 2003). Orthopyroxene porphyroblasts preserve Al contents (on the M1 site =  $y(\text{Opx})$ ) of 0.03 (Table 1). The  $y(\text{Opx})$  isopleths have shallow  $dP/dT$  slopes (Fig. 3d), indicating that they are more sensitive to pressure than temperature. Comparing the observed orthopyroxene compositions with the values predicted on the  $P$ – $T$  pseudosection (Fig. 3d, green-shaded contour) refine conditions in the inferred peak hornblende–clinopyroxene–orthopyroxene–plagioclase–ilmenite–quartz(–K-feldspar–biotite–melt) fields to pressures between 5.7 and 7.3 kbar at 700–855 °C. There is no information on the prograde and retrograde segments of the  $P$ – $T$  path, and therefore the overall shape of the  $P$ – $T$  path is not defined.

Based on the results of phase equilibria modelling and Al-in-orthopyroxene, peak metamorphic conditions are estimated to be 700–855 °C and 5.7 – 7.3 kbar (Fig. 3d), defining an apparent thermal gradient between 100 and 145 °C/kbar

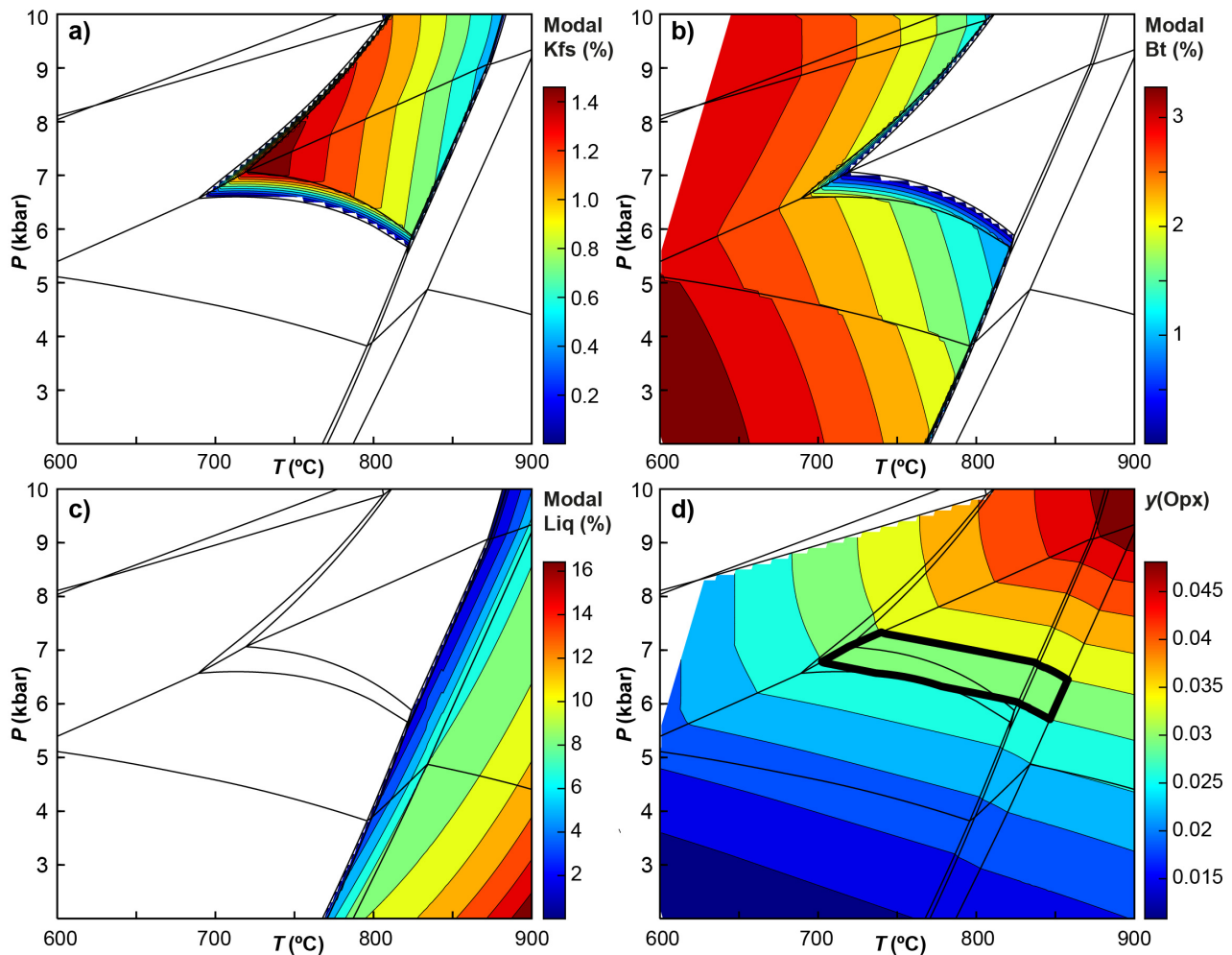


**Figure 3.**  $P$ – $T$  pseudosections with calculated isopleths: a–c) Mode isopleths (mineral proportions; approximately equal to volume percent) for selected minerals in sample 192906: mafic granulite, Burngup (see Figure 2 for labelled  $P$ – $T$  diagram); d) compositional isopleths of Al contents in orthopyroxene (on the M1 site =  $y(\text{Opx})$ ). Thick black lines outline the  $y(\text{Opx})$  values measured from orthopyroxene porphyroblasts (= 0.03) within the inferred peak field(s), and offer the best constraint for the conditions of peak metamorphism

## References

- Cassidy, KF, Champion, DC, Krapež, B, Barley, ME, Brown, SJA, Blewett, RS, Groenewald, PB and Tyler, IM 2006, A revised geological framework for the Yilgarn Craton, Western Australia: Geological Survey of Western Australia, Record 2006/8, 8p.
- Droop, GTR 1987, A general equation for estimating  $\text{Fe}^{3+}$  concentrations in ferromagnesian silicates and oxides from microprobe analyses, using stoichiometric criteria: *Mineralogical Magazine*, v. 51, no. 361, p. 431–435.
- Fielding, IOH, Wingate, MTD, Korhonen, FJ and Rankenburg, K 2021, 198585: pelitic gneiss, Griffins Find; *Geochronology Record 1767*: Geological Survey of Western Australia, 5p.
- Fitzsimons, ICW and Harley, SL 1994, The Influence of Retrograde Cation Exchange on Granulite P–T Estimates and a Convergence Technique for the Recovery of Peak Metamorphic Conditions: *Journal of Petrology*, v. 35, no. 2, p. 543–576.
- Geological Survey of Western Australia 2020, Youanmi, 2020: Geological Survey of Western Australia, Geological Information Series, digital data package.
- Goscombe, B, Foster, DA, Blewett, R, Czarnota, K, Wade, B, Groenewald, B and Gray, D 2019, Neoarchean metamorphic evolution of the Yilgarn Craton: a record of subduction, accretion, extension and lithospheric delamination: *Precambrian Research*, article no. 105441, doi:10.1016/j.precamres.2019.105441.
- Green, ECR, White, RW, Diener, JFA, Powell, R, Holland, TJB and Palin, RM 2016, Activity-composition relations for the calculation of partial melting equilibria in metabasic rocks: *Journal of Metamorphic Geology*, v. 34, no. 9, p. 845–869.
- Holland, T and Blundy, J 1994, Non-ideal interactions in calcic amphiboles and their bearing on amphibole-plagioclase thermometry: *Contributions to Mineralogy and Petrology*, v. 116, no. 4, p. 433–447.
- Holland, TJB and Powell, R 1998, An internally consistent thermodynamic data set for phases of petrological interest: *Journal of Metamorphic Geology*, v. 16, no. 3, p. 309–343.
- Korhonen, FJ, Kelsey, DE, Fielding, IOH and Romano, SS 2020, The utility of the metamorphic rock record: constraining the pressure–temperature–time conditions of metamorphism: Geological Survey of Western Australia, Record 2020/14, 24p.
- Lu, Y, Wingate, MTD, Kirkland, CL, Goscombe, B and Wyche, S 2015a, 198578: pelitic gneiss, Griffins Find; *Geochronology Record 1284*: Geological Survey of Western Australia, 4p.
- Lu, Y, Wingate, MTD, Kirkland, CL, Goscombe, B and Wyche, S 2015b, 198580: quartzite, Griffins Find; *Geochronology Record 1285*: Geological Survey of Western Australia, 5p.
- Lu, Y, Wingate, MTD and Smithies, RH 2018, 224357: biotite metagranodiorite, Phillips River; *Geochronology Record 1550*: Geological Survey of Western Australia, 4p.
- Pattison, DRM, Chacko, T, Farquhar, J and McFarlane, CRM 2003, Temperatures of granulite-facies metamorphism: constraints from experimental phase equilibria and thermobarometry corrected for retrograde exchange: *Journal of Petrology*, v. 44, no. 5, p. 867–900.
- Pearce, MA, White, AJR and Gazley, MF 2015, TCIInvestigator: automated calculation of mineral mode and composition contours for thermocalc pseudosections: *Journal of Metamorphic Geology*, v. 33, no. 4, p. 413–425, doi:10.1111/jmg.12126.
- Powell, R and Holland, TJB 1988, An internally consistent dataset with uncertainties and correlations: 3. Applications to geobarometry, worked examples and a computer program: *Journal of Metamorphic Geology*, v. 6, no. 2, p. 173–204.
- Qiu, Y and McNaughton, NJ 1999, Source of Pb in orogenic lode-gold mineralisation: Pb isotope constraints from deep crustal rocks from the southwestern Archaean Yilgarn Craton, Australia: *Mineralium Deposita*, v. 34, p. 366–381.
- Quentin de Gromard, R, Ivanic, TJ and Zibra, I 2021, Interpreted bedrock geology of the southwest Yilgarn Craton, Geological Survey of Western Australia, in press.
- White, RW, Powell, R, Holland, TJB, Johnson, TE and Green, ECR 2014, New mineral activity-composition relations for thermodynamic calculations in metapelitic systems: *Journal of Metamorphic Geology*, v. 32, no. 3, p. 261–286.
- Wilde, SA 2001, *Jimperding and Chittering metamorphic belts, Western Australia - a field guide*: Geological Survey of Western Australia, Record 2001/12, 24p.
- Wilde, SA and Pidgeon, RT 1987, U–Pb geochronology, geothermometry and petrology of the main areas of gold mineralization in the ‘Wheat Belt’ region of Western Australia: Western Australian Minerals and Petroleum Research Institute; Project 30, Final Report, 171p.

## Links

Metamorphic history introduction document: [Intro\\_2020.pdf](#)

## Recommended reference for this publication

Blereau, ER, Korhonen, FJ and Kelsey, DE 2021, 192906.1: mafic granulite, Burngup; *Metamorphic History Record 4*: Geological Survey of Western Australia, 7p.

Data obtained: 19 May 2020

Date released: 25 June 2021

**This Metamorphic History Record was last modified on 9 June 2021.**

Grid references in this publication refer to the Geocentric Datum of Australia 1994 (GDA94). All locations are quoted to at least the nearest 100 m.

WAROX is GSWA's field observation and sample database. WAROX site IDs have the format 'ABCXXXnnnnnnSS', where ABC = geologist username, XXX = project or map code, nnnnnn = 6 digit site number, and SS = optional alphabetic suffix (maximum 2 characters).

Isotope and element analyses are routinely conducted using the GeoHistory laser ablation ICP-MS and Sensitive High-Resolution Ion Microprobe (SHRIMP) ion microprobe facilities at the John de Laeter Centre (JdLC), Curtin University, with the financial support of the Australian Research Council and AuScope National Collaborative Research Infrastructure Strategy (NCRIS). The TESCAN Integrated Mineral Analyser (TIMA) instrument was funded by a grant from the Australian Research Council (LE140100150) and is operated by the JdLC with the support of the Geological Survey of Western Australia, The University of Western Australia (UWA) and Murdoch University. Mineral analyses are routinely obtained using the electron probe microanalyser (EPMA) facilities at the Centre for Microscopy, Characterisation and Analysis at UWA, and at Adelaide Microscopy, University of Adelaide.

Digital data related to WA Geology Online, including geochronology and digital geology, are available online at the Department's [Data and Software Centre](#) and may be viewed in map context at [GeoVIEW.WA](#).

#### **Disclaimer**

This product uses information from various sources. The Department of Mines, Industry Regulation and Safety (DMIRS) and the State cannot guarantee the accuracy, currency or completeness of the information. Neither the department nor the State of Western Australia nor any employee or agent of the department shall be responsible or liable for any loss, damage or injury arising from the use of or reliance on any information, data or advice (including incomplete, out of date, incorrect, inaccurate or misleading information, data or advice) expressed or implied in, or coming from, this publication or incorporated into it by reference, by any person whatsoever.



© State of Western Australia (Department of Mines, Industry Regulation and Safety) 2021

With the exception of the Western Australian Coat of Arms and other logos, and where otherwise noted, these data are provided under a Creative Commons Attribution 4.0 International Licence. (<http://creativecommons.org/licenses/by/4.0/legalcode>)

#### **Further details of geoscience products are available from:**

Information Centre  
Department of Mines, Industry Regulation and Safety  
100 Plain Street  
EAST PERTH WA 6004  
Telephone: +61 8 9222 3459 | Email: [publications@dmirs.wa.gov.au](mailto:publications@dmirs.wa.gov.au)  
[www.dmirs.wa.gov.au/GSWApublications](http://www.dmirs.wa.gov.au/GSWApublications)